catalysts

MDPI

Review

Titanium-Dioxide-Based Visible-Light-Sensitive Photocatalysis: Mechanistic Insight and Applications

Shinya Higashimoto

Department of Applied Chemistry, Faculty of Engineering, Osaka Institute of Technology, 5-16-1 Omiya, Asahi-ku, Osaka 535-8585, Japan; shinya.higashimoto@oit.ac.jp; Tel.: +81-(0)6-6954-4283

Received: 15 January 2019; Accepted: 14 February 2019; Published: 22 February 2019

Abstract: Titanium dioxide (TiO_2) is one of the most practical and prevalent photo-functional materials. Many researchers have endeavored to design several types of visible-light-responsive photocatalysts. In particular, TiO_2-based photocatalysts operating under visible light should be urgently designed and developed, in order to take advantage of the unlimited solar light available. Herein, we review recent advances of TiO_2-based visible-light-sensitive photocatalysts, classified by the origins of charge separation photo-induced in (1) bulk impurity (N-doping), (2) hetero-junction of metal (Au NPs), and (3) interfacial surface complexes (ISC) and their related photocatalysts. These photocatalysts have demonstrated useful applications, such as photocatalytic mineralization of toxic agents in the polluted atmosphere and water, photocatalytic organic synthesis, and artificial photosynthesis. We wish to provide comprehension and enlightenment of modification strategies and mechanistic insight, and to inspire future work.

Keywords: Titanium dioxide (TiO_2); visible-light-sensitive photocatalyst; N-doped TiO_2; plasmonic Au NPs; interfacial surface complex (ISC); selective oxidation; decomposition of VOC; carbon nitride (C_3N_4); alkoxide; ligand to metal charge transfer (LMCT)

1. Introduction

Titanium dioxide (TiO_2) is one of the most practical and prevalent photo-functional materials, since it is chemically stable, abundant (Ti: 10th highest Clarke number), nontoxic, and cost-effective. In recent years, a great deal of attention has been directed towards TiO_2 photocatalysis for useful applications such as photocatalytic mineralization of toxic agents in the polluted atmosphere and water, photocatalytic organic synthesis, and artificial photosynthesis [1–20].

The TiO_2 involving Ti^{3+} sites that are oxygen-deficient at the impurity level exhibits n-type semiconductor. The photocatalytic activities of TiO_2 strongly depend on crystal structures (anatase, brookite, and rutile), crystallinity, crystalline plane, morphology, particle sizes, defective sites, and surface OH groups. The valence band (V.B.) and conduction band (C.B.) of TiO_2 consist of O 2p and Ti 3d orbitals, respectively, and their band gap (forbidden band) is circa ~3.0–3.2 eV (~410–380 nm). Photo-irradiation ($h\nu$ > 3.2 eV) of the TiO_2 photocatalyst leads to band gap excitation, resulting in charge separation of electrons into the C.B. and the holes in the V.B. These photo-formed electrons and holes simultaneously work as electron donors and acceptors, respectively, on the photocatalyst surface, thus enabling the photocatalytic reactions. Details are given in other articles and reviews [21–25]. UV light reaching the earth surface represents only a very small fraction (4%) of the solar energy available. Therefore, many researchers have endeavored to design several types of visible-light-responsive photocatalyst. In particular, TiO_2-based photocatalysts operating under visible light should be urgently designed and developed, in order to take advantage of the unlimited solar light available.

In the late 1990s, Anpo et al. first reported that TiO_2 doped with Cr, V, and Fe cations by ion implantation operates under visible light irradiation. They exhibited red shift of the band-edge of the

TiO_2, resulting in decomposition of NO into N_2, O_2, and N_2O [26]. This work accelerated subsequent works for the design and development of visible-light-responsive photocatalysts. Recently, much attention has been paid to visible-light-responsive TiO_2 prepared by: doping with nitrogen (N), carbon (C), and sulfur (S) ions etc.; surface plasmonic effects with Au or Ag nanoparticles (NPs); the interfacial surface complex (ISC); coupling with visible-light-sensitive hetero-semiconductors (cadmium sulfide, carbon nitride etc.); and dye-sensitized photocatalysts. In fact, some photocatalysts are considered to work under similar principles.

Along these backgrounds, this review focuses on the recent advances of the visible-light-sensitive TiO_2 photocatalyst. These advances have been classified by the origin of charge separation photo-induced in (1) the bulk impurity (N-doping), (2) hetero-junction of metal (Au NPs), and (3) the interfacial surface complex (ISC) (See Figure 1). They have been well characterized by several spectroscopic techniques, and applied for mineralization of volatile organic compounds (VOC), water splitting to produce H_2, and fine organic synthesis.

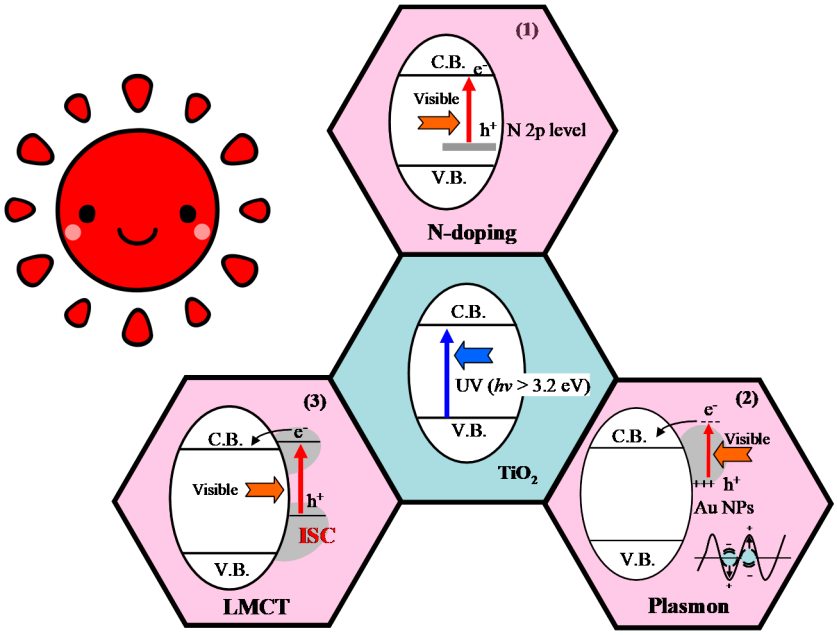

Figure 1. Visible-light-sensitive TiO_2 photocatalyst modified by (**1**) nitrogen-doping, (**2**) plasmonic Au nanoparticles (NPs), and (**3**) interfacial surface complex (ISC).

2. Nitrogen-doped TiO_2 Photocatalysts

In 1986, Sato and co-workers first explored the photocatalytic activity of nitrogen-doped TiO_2 (N-doped TiO_2) photocatalysts for the oxidation of gaseous ethane and carbon monoxide [27]. They found that N-doped TiO_2 photocatalyst exhibited a superior photocatalytic activity to pure TiO_2 under visible light irradiation. Later, in 2001, Asahi et al. demonstrated visible-light-induced complete photo-oxidation of gaseous CH_3CHO (one of VOCs) to CO_2 with an N-doped TiO_2 photocatalyst [28]. In this section, fundamental synthetic routes, characterizations, and application of photocatalytic reactions are highlighted.

2.1. Synthesis of N-doped TiO_2 Photocatalyst

N-doped TiO_2 was prepared by employing several procedures and materials. Details are given in Reference [13]. Preparation methods for N-doped TiO_2 photocatalysts can be classified into two categories: dry processes and wet processes.

2.1.1. Dry Processes

Typically, N-doped TiO_2 powder can be prepared by the nitrification of TiO_2 in an ammonia (NH_3) gas flow at high temperature [28,29]. The amount of N doping into the TiO_2 can be controlled by annealing temperatures in the range of 550−600 °C under an NH_3 flow. However, a large number of O vacancies are introduced into the N-doped TiO_2 with increasing annealing temperature, since the NH_3 decomposes into N_2 and H_2 at high temperature, and TiO_2 is simultaneously reduced by H_2 [30]. Figure 2 shows schematics of N-doping into TiO_2, accompanied by the formation of oxygen vacancies to exhibit the n-type semiconductor.

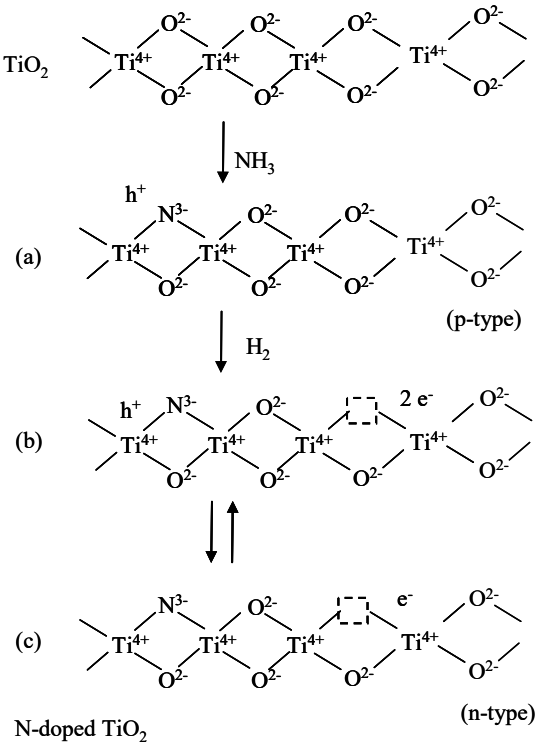

Figure 2. When the N^{3-} is replaced with lattice O^{2-} ions in the TiO_2 lattice, the hole (h^+) is formed in order to compensate for the charge balance (p-type semiconductor) (a). However, an oxygen vacancy is produced by the reduction with H_2, which is formed by the decomposition of NH_3 to produce an oxygen vacancy and excess electrons (b). As a consequence, N^{3-} doped into TiO_2 (N-doped TiO_2) involves electrons located at N 2p and Ti 3d sites at impurity levels (n-type semiconductor) (c).

2.1.2. Wet Processes

A sol-gel method can be employed for the preparation of N-doped TiO_2 powder. Typically, NH_3 aq. (NH_4OH) is added to a solution of titanium (IV) isopropoxide (TTIP) [31–33] to form titanium hydroxide involving N-species. The precipitate was dried, followed by calcination at ~400–450 °C in air to obtain a yellowish TiO_2 powder.

2.2. N-states in N-doped TiO_2

One of the major concerns is to understand the physico-chemical nature of the N species in N-doped TiO_2, which are responsible for the visible light sensitivity. They were characterized by density functional theory (DFT) calculations, X-rap photoelectron spectroscopy (XPS), Ultraviolet-visible (UV-vis) and electron paramagnetic resonance (EPR) spectroscopy.

2.2.1. DFT Calculations

DFT calculations demonstrated the electronic structures of the N-doped TiO_2 photocatalyst (see Figure 3). The substitution of N with lattice O of the N-doped TiO_2 exhibits band gap narrowing (circa 0.1 eV) caused by mixing orbitals of N 2p with O 2p, resulting in the negative shift of the valence band edge. On the other hand, the interstitial N is localized to impurity states (N 2p levels) above the V.B. (circa 0.7 eV) in the mid-band gap. Therefore, the oxidation power of photo-induced holes on the N 2p is lower than on the O 2p in the TiO_2 lattice.

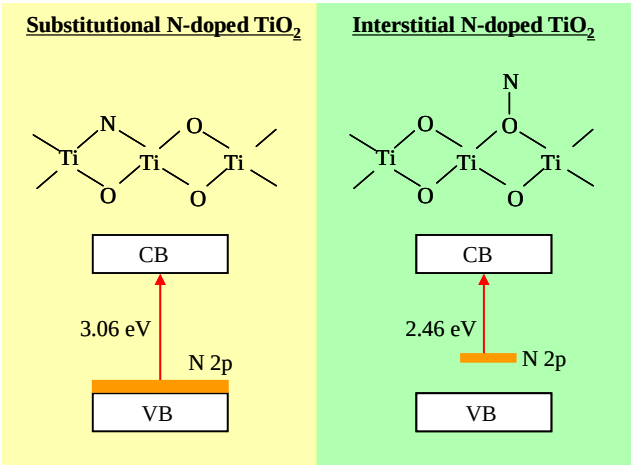

Figure 3. Schematic illustration of structures and their corresponding energy bands for substitutional and interstitial N species in the N-doped TiO_2, together with photo-induced electronic processes.

2.2.2. XPS Spectra

XPS analysis can confirm the oxidative states of the N species and bonding states in the N-doped TiO_2 (See Figure 4I). N 1s XPS peaks at a binding energy in the range of ~396–400 eV showed different oxidative states of the N species. By the combination of the DFT calculations [31], it was identified that the N 1s XPS peaks at ~396–397 eV are due to the substitution of N with the lattice O of TiO_2 [13,34], while those at ~399–400 eV are due to the interstitial N in the form of NO_x or NH_x [13,31,35,36].

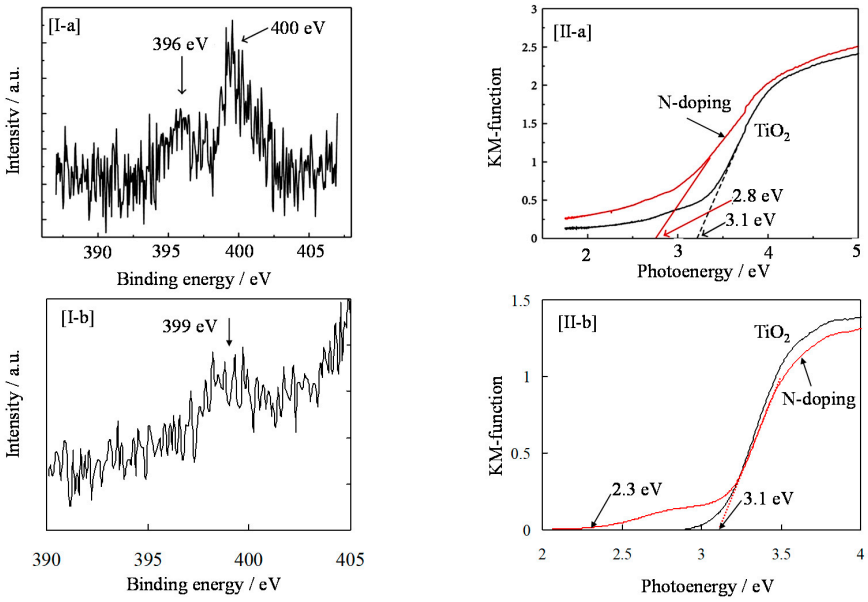

Figure 4. XPS [I] and UV-vis absorption spectra [II] of (a) N-doped TiO_2 nanoball film [34], and (b) N-doped TiO_2 prepared by the sol-gel method [36].

2.2.3. Optical Properties

The UV-vis absorption spectra of the N-doped TiO_2 are shown in Figure 4II. The N-doped TiO_2 with the substitution of N exhibited band gap narrowing from 3.1 to 2.8 eV. On the other hand, the N-doped TiO_2 prepared by the sol-gel method exhibited visible light absorption up to 540 nm (2.3 eV), due to the electronic transition from localized N doping level to the C.B. of the TiO_2, while band-narrowing was not observed. These results are in good agreement with the DFT calculations.

2.2.4. Electron Paramagnetic Resonance (EPR) Spectra

N species in the N-doped TiO_2 are present at either diamagnetic (N^-) or paramagnetic ($N^\bullet$) bulk centers, which are responsible for the visible light sensitivity [31,37]. The EPR measurements can detect the paramagnetic ($N^\bullet$) bulk centers (see Figure 5). One type, of three lines with a hyperfine tensor (g = 2.006 and A = 32.0 G) splitting by nuclear spin of nitrogen (I = 1), was observed. The signal intensity of $N^\bullet$ radicals increased when the light was turned on, while the signal intensity significantly decreased when the light was turned off. In general, the paramagnetic interaction between N species and O_2 makes EPR signals disappear. However, they were remarkably enhanced in the presence of O_2 under $\lambda > 420$ nm, while its signal intensity still remained to some extent even after the light was turned off. These results suggest that N-species are located in bulk inside the TiO_2, and visible light irradiation of the N-doped TiO_2 exhibits effective charge separation to form holes ($N^\bullet$ radicals) and electrons, which participate in the oxidation and reduction of reactant molecules, respectively.

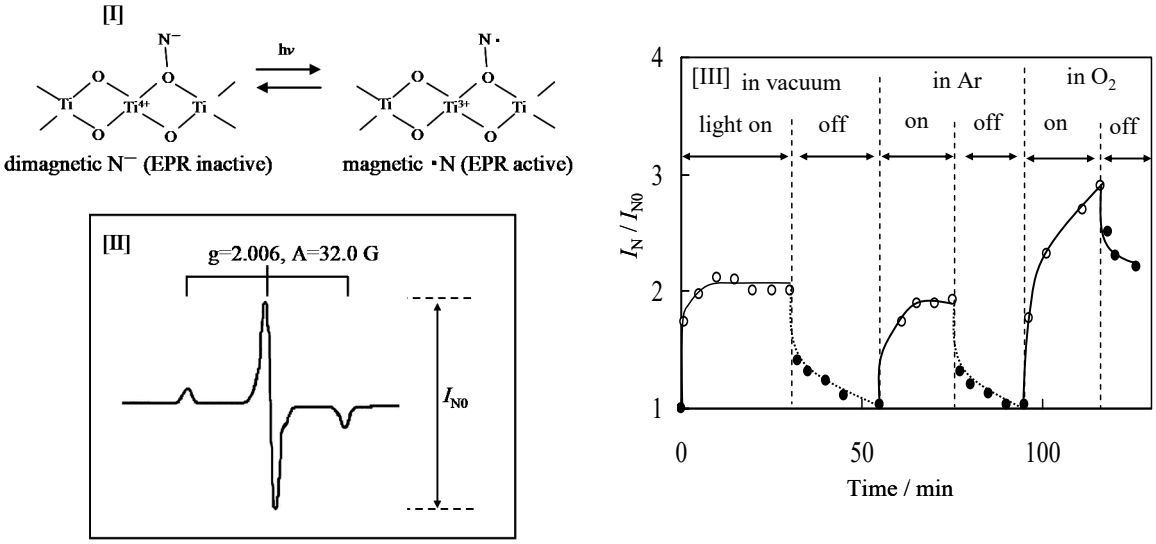

Figure 5. Schematic illustration of [I] formation of paramagnetic ·N by the excitation of diamagnetic N^- species. Electron paramagnetic resonance (EPR) signal [II] of ·N radicals on N–TiO_2, and the relative signal intensity of I_N/I_{N0} [III] under vacuum, in the presence of argon (Ar) or O_2 (400 Pa) [37]. I_{N0} and I_N show the intensity due to ·N radicals at the initial and measured time, respectively.

2.2.5. Photo-Electrochemical Properties

Nakamura et al. investigated the photo-electrochemical oxidation power of the N-doped TiO_2 by employing several electron donors [38]. Figure 6 shows that the photo-induced hole on the N 2p level can directly oxidize only I^- ions under visible light illumination, while I^-, SCN^-, Br^-, and H_2O are oxidized by the hole on the V.B. under UV light illumination. Therefore, the oxidation power of the holes induced on the N 2p level is lower than that of those on the O 2p on the V.B. Tang et al. studied the dynamics of photogenerated electrons and holes on the N-doped TiO_2 using transient absorption spectroscopy [39]. They concluded that the lack of activity of nanocrystalline N-doped TiO_2 film for photocatalytic water oxidation is due to rapid electron–hole recombination.

On the other hand, Higashimoto et al. investigated the photo-electrochemical reduction power of the N-doped TiO_2 (see Figure 7) [33]. When the N-doped TiO_2 was photo-excited under visible light irradiation, the photo-induced electrons were accumulated on the oxygen vacancies of TiO_2. Subsequently, when various kinds of redox species as electron acceptors were introduced into the photo-charged N–TiO_2, the accumulated electrons could reduce O_2 molecules, Pt^{4+}, Ag^+, and Au^{3+} ions, but not MV^{2+}, H^+, and Cu^{2+} ions. In principle, the N-doped TiO_2 has the potential to reduce H^+/H_2, but many oxygen vacancies involved in the bulk TiO_2 could influence the drastic charge recombination. In particular, photo-induced electrons trapped at the oxygen vacancies (mainly γ region) could reduce O_2 molecules to form such active oxygen species as hydrogen peroxide (H_2O_2), resulting in further oxidation of organic substrates.

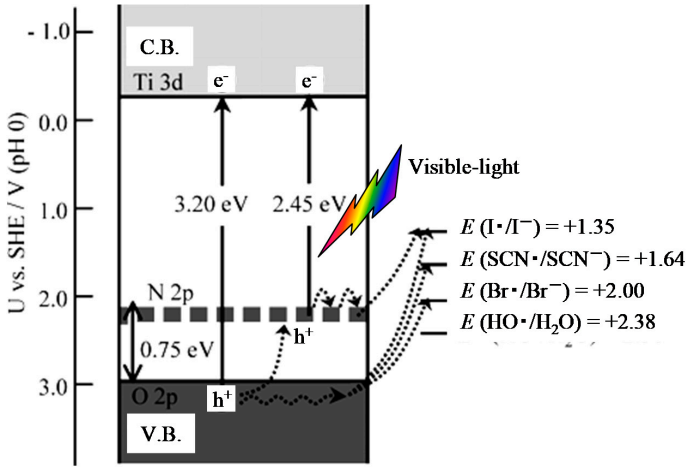

Figure 6. Schematic illustration of proposed energy bands for the N-doped TiO_2, together with some photo-induced electronic processes. *E*: equilibrium redox potentials for one electron transfer [38].

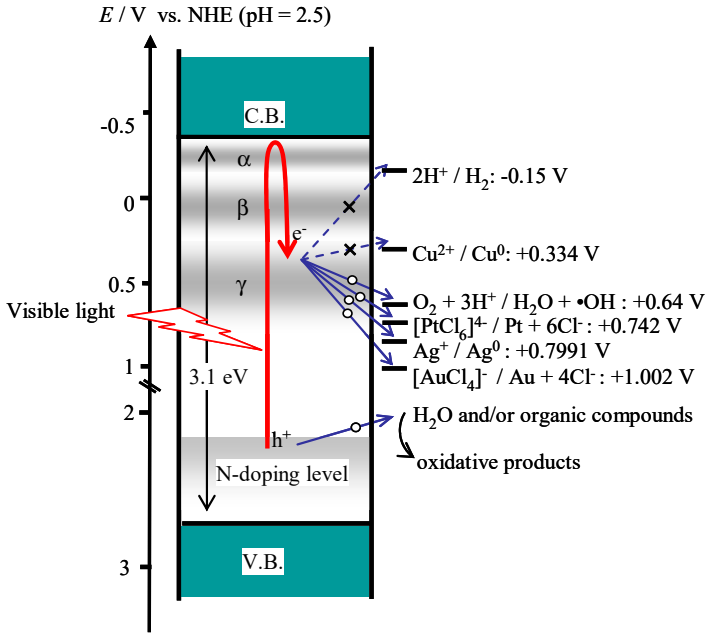

Figure 7. Energy levels for sub-band structures of N-doped TiO_2 and photo-induced charge transfer into various kinds of redox species under visible light irradiation. The energy levels of sub-bands at the α, β, and γ potential regions (oxygen vacancies) and N-doping levels are also shown. Oxygen vacancies were estimated from the photo-electrochemical measurements. Signs of circle and cross stand for energetically favorable and unfavorable electron transfers, respectively [33].

2.3. Application to Photocatalytic Decomposition of Volatile Organic Compounds (VOC)

Time profile for the photocatalytic decomposition of gaseous acetaldehyde on the N-doped TiO_2 is shown in Figure 8. The N-doped TiO_2 exhibited photocatalytic activity 5 times greater than TiO_2 under visible light irradiation, while they exhibited similar activities under UV light irradiation [28].

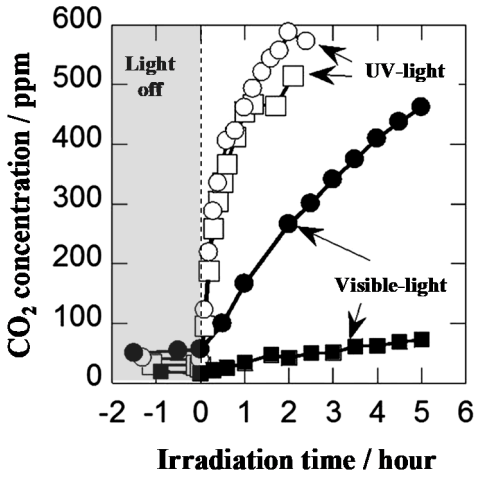

Figure 8. Photocatalytic decomposition of gaseous acetaldehyde on the N-doped TiO_2 photocatalyst. Evolved CO_2 concentration (○, ●, N-doped TiO_2; □, ■, TiO_2) [28].

Table 1 shows that the N-doped TiO_2 exhibited photocatalytic activity for the decomposition of several kinds of VOC into CO_2 under visible light irradiation ($\lambda > 420$ nm). It was observed that the N-doped TiO_2 exhibited photocatalytic activity for the decomposition of aldehydes, but little activity for alcohol, acid, ketone, and halogene compounds. The vanadium species was deposited on the N-doped TiO_2 (VCl_3/N-doped TiO_2) by impregnation method. As shown in Table 1, VCl_3/N-doped TiO_2 showed higher photocatalytic activity for the decomposition of all VOC, in particular, acetic acid or acetone by ~13–16 times more than N-doped TiO_2. Therefore, it was confirmed that vanadium species worked as the effective co-catalyst.

Table 1. Yields of CO_2 for the photocatalytic decomposition of various kinds of volatile organic compounds (VOC) in aqueous solutions with N–TiO_2 and VCl_3/N-doped TiO_2 under visible light irradiation ($\lambda > 420$ nm) for 3 h [40].

Entry	Reactant Molecules	Yields of CO_2/μmol	
		N-doped TiO_2	VCl_3/N-doped TiO_2
1	methanol [a]	0.2	1.1
2	ethanol [a]	0.3	0.5
3	formaldehyde [a]	4.6	21.6
4	acetaldehyde [a]	4.1	35.0
5	formic acid [a]	0.7	4.8
6	acetic acid [a]	1.2	17.0
7	acetone [a]	0.7	11.4
8	ethyl acetate [a]	1.3	10.6
9	dichloromethane [b]	2.4	4.1
10	trichloromethane [b]	1.5	4.1
11	1, 1-dichloroethane [b]	0.7	4.8
12	trans-1, 2-dichloroethylene [b]	1.0	5.7

Concentrations of VOC are (a) 0.5 M and (b) 50 mM.

Furthermore, effects of co-catalysts (48 metal ions using nitrate, sulfate, chloride, acetate, and oxide precursors) deposited on the N-doped TiO_2 for the photocatalytic activities were examined (See Figure 9) [40]. The bars marked in yellow exhibited higher photocatalytic activities than the N-doped TiO_2 by itself. In particular, N-doped-TiO_2-deposited Cu, Fe, V, and Pt oxides exhibited high photocatalytic activities. The local structures of the co-catalysts were characterized by XPS. It was observed that Cu loaded N-doped TiO_2 involves cuprous oxide (Cu_2O) or Cu hydroxides, Fe loaded N-doped TiO_2 involves clusters containing Fe–O bonds or Fe^{2+} hydroxide [41], and Pt loaded N-doped TiO_2 involves Pt^{4+}/Pt^{2+} species [36]. The redox potentials of co-catalysts such as V (+IV/+V), Fe (+II/+III), Cu (+I/+II), and Pt (+III/+IV) were in the range of circa +0.6 to +1.0 V vs. SHE, while the multi-electron reduction of O_2 leads to the formation of active oxygen species via $O_2 + 2H^+ + 2e^-$ / H_2O_2 (E_0 = +0.687 V vs. SHE). Therefore, the co-catalysts, such as Pt, Fe, Cu, and V species, enhance the photocatalytic activity due to the effective electron transfer to O_2 (O_2 reduction), resulting in the formation of active oxygen species.

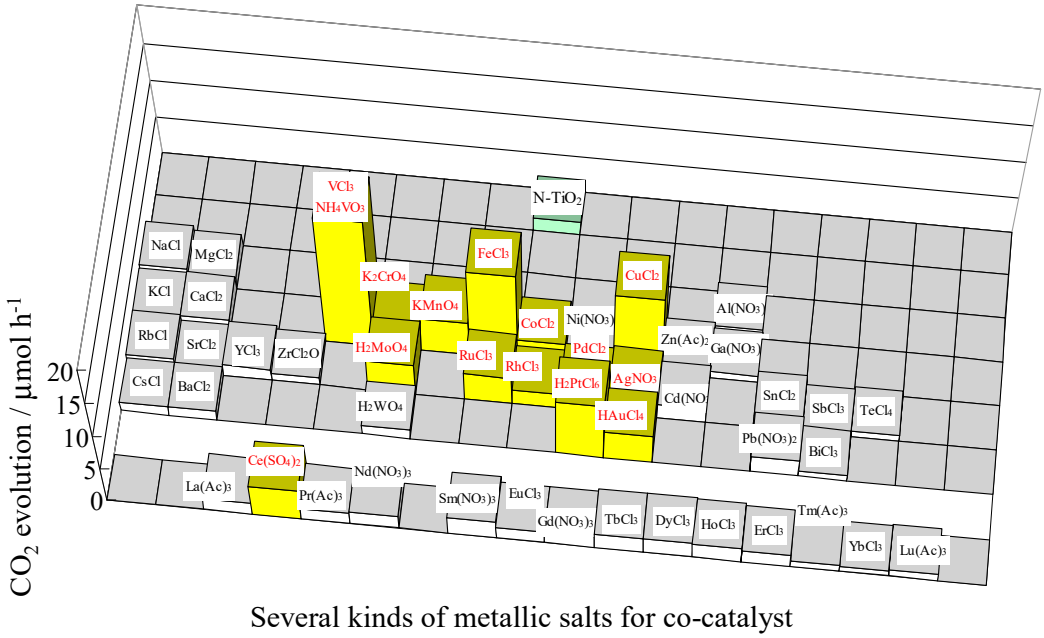

Figure 9. Photocatalytic activities for the decomposition of acetic acid under visible light irradiation ($\lambda > 420$ nm) on N-doped TiO_2, modified by various kinds of metal species as co-catalysts. Each metal salt used in this study is shown [40].

2.4. C_3N_4-Modified TiO_2 Compared with N-doped TiO_2

Several nitrogen sources such as urea, cyanamid, cyanuric acid, and melamine were employed for the preparation of N-containing TiO_2 photocatalyst, i.e., the TiO_2 surface is modified with polymerized carbon nitride (C_3N_4) [42–51]. The structures of the C, N-species strongly depend on their concentrations. If the C, N species are present in only a small amount, they act as a molecular photosensitizer. At higher amounts they form a C_3N_4 crystalline semiconductor, which chemically binds to TiO_2. The C_3N_4–TiO_2 was systematically synthesized by thermal condensation of cyanuric acid on the TiO_2 surface [51]. In fact, H_2 was evolved from TEA aq. on the C_3N_4–TiO_2 photocatalyst under visible light irradiation, while the N-doped TiO_2 did not exhibit H_2 production. From characterization of C_3N_4–TiO_2 by Fourier transformed-infrared (FT-IR), XPS, electrochemical measurements, and DFT calculations, the band structures and photo-induced charge separation mechanisms were demonstrated (Figure 10). The C_3N_4–TiO_2 was found to exhibit photo-induced charge separation through the hetero-coupling of semiconductors between C_3N_4 and TiO_2 on the surface. On the other hand, N-doped TiO_2 was photo-sensitized by bulk impurity of the N-doping. It can be assumed that many

oxygen vacancies promoted the charge recombination, resulting in weak reduction power in the N-doped TiO_2.

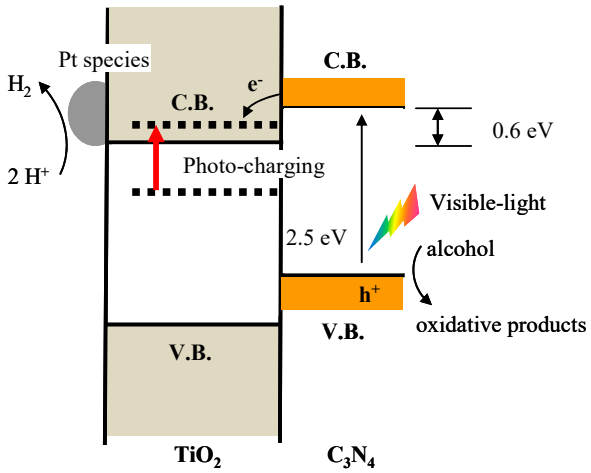

Figure 10. Photo-induced charge separation on the C_3N_4 deposited TiO_2 surface [51].

3. Plasmonic Au NPs Modified TiO_2

3.1. What Is Localized Surface Plasmon Resonance (LSPR)?

Localized surface plasmon resonance (LSPR) is an optical phenomenon generated by light when it interacts with conductive nanoparticles (NPs) that are smaller than the incident wavelength. The LSPR is induced by the collective oscillations of delocalized electrons in response to an external electric field. The resonance wavelength strongly depends on the size and shape of the NPs, the interparticle distance, and the dielectric property of the surrounding medium. The Au and Ag NPs exhibit unique plasmon absorption [52,53]. The plasmonic Ag NPs are considered to be unstable under illumination, and could be applicable to multi-colored rewritable devices. In this section, we focused on stable plasmonic Au NPs exploited for a visible-light-sensitive photovoltaic fuel cell or photocatalyst [54,55].

3.2. Preparation and Characterization of Au–TiO_2 Photocatalyst

3.2.1. Photodeposition (PD) Methods

By using the photocatalysis of TiO_2, metallic Au was deposited on the TiO_2 surface, accompanied by the oxidation of methanol [56,57] or ethanol [58]. Typically, TiO_2 powder was suspended in a 50 vol. % aqueous methanol in the presence of $HAuCl_4 \cdot 6H_2O$, purged of air with argon. The suspension was photoirradiated with UV light under magnetic stirring. The temperature of the suspension during photoirradiation was maintained at 298K. The Au/TiO_2 photocatalyst was centrifuged, washed with distilled water, dried at 393K, and ground in an agate mortar.

3.2.2. Colloid Photodeposition Operated in the Presence of a Hole Scavenger (CPH)

Colloidal Au NPs were prepared using the method reported by Frens [59]. In brief, mixtures of an aqueous tetrachloroauric acid ($HAuCl_4$) solution and sodium citrate were heated and boiled for 1 h. The color of the solution changed from deep blue to deep red. The citrate plays a role in the reduction of Au ions, and the capping agent in suppressing the aggregation of Au NPs. The suspension of TiO_2 in an aqueous solution of colloidal Au NPs and oxalic acid was then photo-irradiated at $\lambda > 300$ nm at 298 K under argon (Ar). The solids were recovered, washed, and dried to produce Au–TiO_2. Details are given in Reference [60].

3.2.3. Deposition Precipitation (DP) Method

Deposition–precipitation (DP) methods were employed for the deposition of a gold (III) species on the TiO_2 surface [61,62]. The $[AuCl(OH)_3]^-$, main species present at pH 8, adjusted by NaOH aq., reacts with hydroxyl groups of the TiO_2 surface to form a grafted hydroxyl–gold compound. The catalyst was then recovered, filtered, washed with deionized water, and dried. Finally, the powder was calcined at ~473–673 K in air.

3.2.4. Characterization of the Au–TiO_2 Photocatalyst

The Au–TiO_2 photocatalysts were typically characterized by the transmittance electron microscope (TEM) for the particle sizes, and UV-vis absorption for optical properties (See Table 2).

Table 2. Particle sizes of Au nanoparticles (NPs) and optical properties of the Au–TiO_2 prepared by several techniques.

Entry	Au Deposition Methods	Particle Sizes/nm	Top Peak/nm	Ref.
1	PD	~10–60	~530–610	[56–58]
2	CPH	~12–14	~550–560	[60,63–66]
		13	~550–620	[67]
3	DP	~2–6	~550–560	[61]
		< 5	550	[68–70]

Kowalska et al. [56,57] reported that Au–TiO_2 photocatalysts with different Au particle sizes (~10–60 nm) were prepared by photo-deposition (entry 1). The particle sizes of Au strongly depend on the particle sizes of the TiO_2 polycrystalline structure. The top peak of plasmonic absorption was in the range of ~530–610 nm, depending on the particle sizes of the Au NPs. Tanaka and Kominami et al. [60,63–66] reported unique CPH methods for the preparation of Au-TiO_2 (entry 2). The particle sizes were uniformed to be ~12–14 nm, which exhibits plasmonic absorption at ~550–560 nm. Thus, colloidal Au NPs were successfully loaded onto TiO_2 without change in the original particle size. Furthermore, the top peak of Au plasmon absorption was found to extend towards 620 nm by simple calcinations of the samples. This phenomenon is due to high contact area between TiO_2 and Au NPs without change of particle size [66]. Additionally, Naya et al. [67,68] and Shiraishi et al. [69] employed precipitation deposition methods to deposit small Au NPs (~2–6 nm) on TiO_2 (entry 3).

3.3. Application of LSPR of Au–TiO_2 to Several Photocatalytic Reactions

Au NPs deposited on TiO_2 have been used as visible-light-responsive photocatalysts for several chemical reactions: decomposition of VOCs, selective oxidation of an aromatic alcohol, direct water splitting, H_2 formation from sacrificial aqueous solutions, and reduction of organic compounds (see Table 3). Several research groups concluded that photocatalytic activities are induced by LSPR of the Au NPs. Some research indicates that small Au NPs (~5 nm) effectively work for the reactions [61,69]. Tanaka and Kominami et al. suggest that two types of Au particles of different sizes loaded onto TiO_2 exhibit different functionalities. That is, the larger Au particles contribute to strong light absorption, and the smaller Au particles act as a co-catalyst for H_2 evolution [63].

Table 3. Applications to several photocatalytic reactions on the Au–TiO_2 photocatalyst.

Entry	Photocatalytic Reactions	Au Deposition Methods	References
1	oxidations of 2-propanol and ethanol	PD	[56–58]
	oxidation of formic acid	CPH	[60]
2	oxidation of thiol to disulfide	DP	[67]
	oxidation of amine to imine	DP	[68]
	oxidation of aromatic alcohol to aldehyde	CPH	[66]
		DP	[69]
	oxidation of benzene to phenol	PD	[70]
3	H_2 formation from alcohols	CPH	[63,71]
	water splitting into H_2 and O_2	DP	[61]
		CPH	[64,72]
4	reduction of nitrobenzene to aniline	CPH	[65]

3.4. Application to a Photovoltaic Fuel Cell Operating under Visible Light Irradiation

The Au–TiO_2 films were found to exhibit the behavior of a photovoltaic fuel cell [54,55]. An anodic photocurrent was yielded on the Au−TiO_2 film as the visible light was irradiated, while the current was observed neither on a TiO_2 film under visible light irradiation, nor on the Au−TiO_2 film when the light was turned off. The short-circuit photocurrent density (J_{sc}) was strongly influenced by kinds of donors, and the photocurrent efficiency was maximized in the presence of Fe^{2+} ions. Furthermore, the photocurrent action spectra were closely fitted with the absorption spectrum of the Au NPs deposited on the TiO_2 film (See Figure 11).

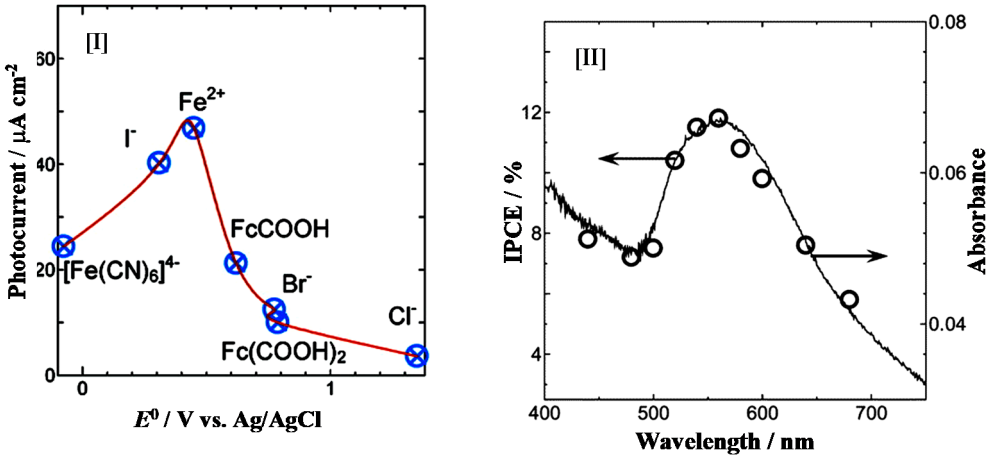

Figure 11. Short-circuit photocurrent densities [I] vs. apparent formal potential of different donors on the Au−TiO_2 photoanode in acetonitrile/ethylene glycol (v/v 60/40) containing 0.1 M $LiNO_3$ and 0.1 M donors; IPCE [II] of the Au−TiO_2 film in a N_2-saturated acetonitrile and ethylene glycol (v/v: 60/40) solution containing 0.1 M $FeCl_2$ and 0.05 M $FeCl_3$ [55].

3.5. Mechanisms of Charge Separation

The mechanism for the Au plasmon-induced charge separation is shown in Figure 12. Visible light irradiation generates the photo-excited state of the Au NPs by LSPR. The photo-excited electrons are injected into the C.B. of TiO_2, while the holes abstracted electrons from a donor in the solution. The Au NPs behave like an intrinsic semiconductor, and the Fermi levels of Au NPs and TiO_2 are leveled out, resulting in the formation of Schottky barrier at Au–TiO_2 junctions. This band model seems to be similar with dye-sensitized photo-anodic electrodes.

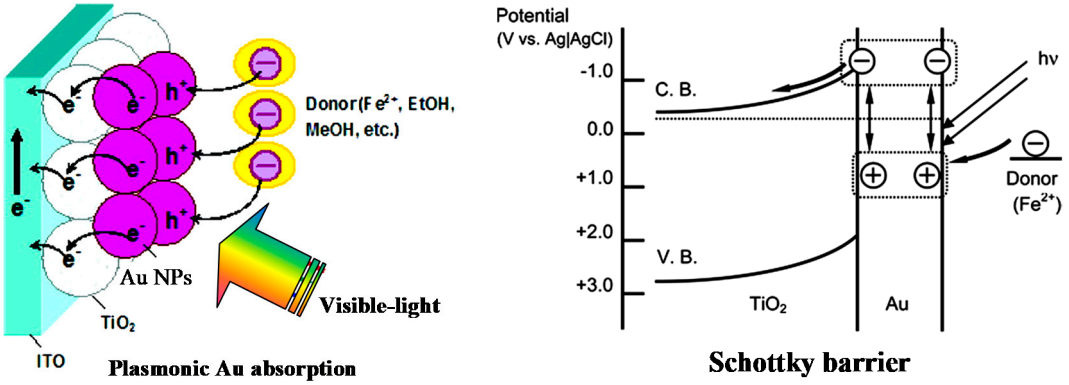

Figure 12. Schematic illustration [I] and its energy band levels [II] for the photo-induced charge separation on the Au–TiO_2 in the presence of donors [55].

Recently, Furube et al. studied the plasmon-induced charge transfer mechanisms between Au NPs and TiO_2 by means of femtosecond visible pump/infrared probe transient absorption spectroscopy [73]. The electron transfer from the Au NPs to the C.B. of TiO_2 was confirmed to occur within 50 fs, and that the electron injection yielded 20–50% upon 550 nm laser excitation.

4. Photo-Induced Interfacial Charge Transfer

4.1. Dye-Sensitized TiO_2 Photocatalysis

Dye sensitized TiO_2 photocatalysis was studied in the late 1990s. The Ru complex, $[Ru(bipy)_3]^{2+}$ grafted on the TiO_2 surface exhibits visible light absorption [74,75]. In this system, the excitation of the Ru complex induces electron transfer via metal–ligand charge transfer (MLCT). The photo-induced electrons are then transferred onto TiO_2, resulting in photocatalytic water splitting to produce H_2. The platinum-chloride-modified TiO_2 system was reported by Kisch et al. [76,77]. Photo-irradiation of Pt(IV) chloride exhibits visible-light absorption to generate the active center, $(Pt^{4+}(Cl^{-})_4 + h\nu \rightarrow Pt^{3+}Cl^{0}(Cl^{-})_3$. The photo-induced electrons are transferred from Pt^{3+} to C.B. of TiO_2 as reductive sites, while the Cl^0 work as the oxidative sites, resulting in the redox photocatalytic reactions. Important strategies to develop these types of photocatalysts are to design robust sensitizers adjusted with HOMO-LUMO levels.

4.2. Visible-Light-Responsive TiO_2 Photocatalyst Modified by Phenolic Organic Compounds

Strong interaction of phenolic groups in organic compounds with Ti–OH of the TiO_2 surface probably forms two types of interfacial surface complexes (ISC, Figure 13I), which exhibits visible light absorption via LMCT. The photocatalysis of the ISC is strongly influenced by the electronic structures of the ISC (Figure 13II): the ISC with EWG exhibits strong oxidizability under visible light irradiation, and it can favorably oxidize the TEA, together with H_2 evolution from deaerated TEA aqueous solutions [78]. The visible light response of the ISC is attributed to electronic excitation from the donor levels (0.7 V above V.B.) to the C.B. of TiO_2 (see Figure 14). Therefore, the electronic structures of sensitizers strongly influence the photocatalytic activities. Ikeda et al. [79] demonstrated that a TiO_2 photocatalyst modified with 1,1′-binaphthalene-2,2′-diol ($bn(OH)_2$) exhibited photocatalytic H_2 evolution from deaerated TEA aq. under visible light irradiation. Kamegawa et al. [80] designed a 2, 3-dihydroxynaphthalene (2,3-DN)-modified TiO_2 photocatalyst for the reduction of nitrobenzene to aminobenzene under visible light irradiation.

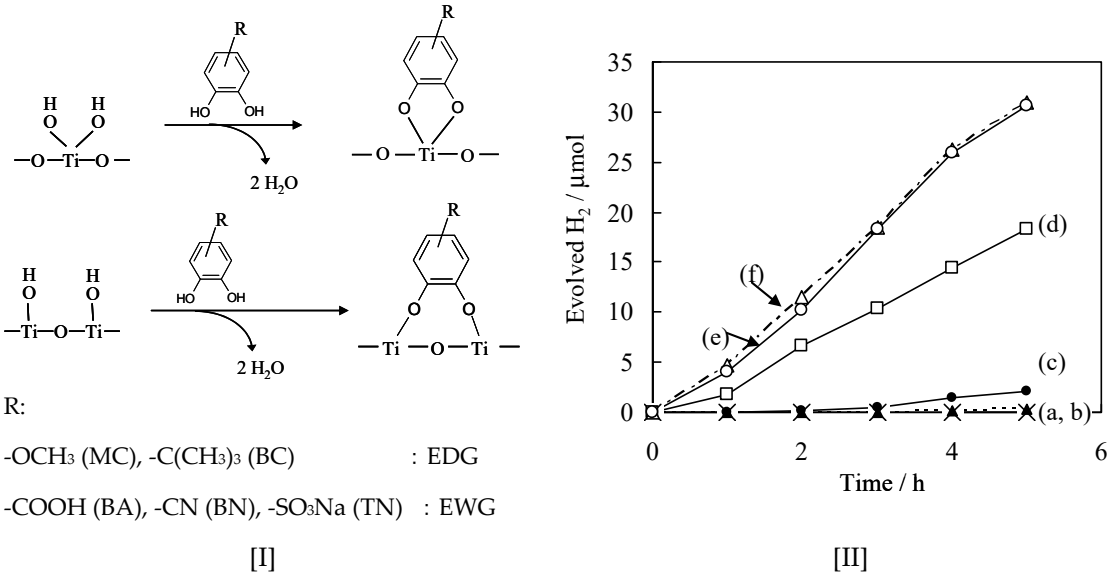

Figure 13. Schematic illustration for the formation of two types of ISCs [I], and photocatalytic H_2 evolution [II] from aq. TEA (10 vol. %) on (a) BC/TiO_2, (b) MC/TiO_2, (c) CA/TiO_2, (d) BA/TiO_2, (e) BN/TiO_2, and (f) TN/TiO_2 [78]. BC: 4-*t*-butyl catechol, MC: 3-methoxy catechol, CA: catecol, BA: 2,3-dihydroxy benzoic acid; BN: 3,4-dihydroxy benzonitrile; TN: tiron.

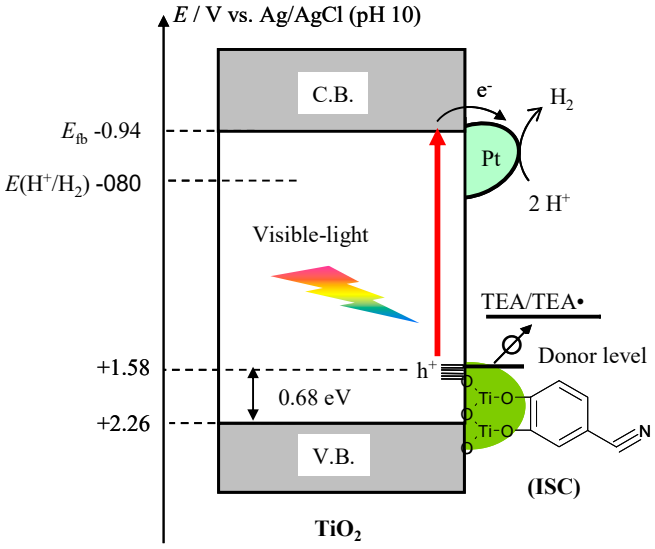

Figure 14. Schematic illustration of photo-induced charge separation on the BN/TiO_2 for H_2 evolution from TEA aq. in the presence of Pt as co-catalyst under visible light irradiation [78].

On the other hand, the phenolic compounds were degraded on the TiO_2 in the presence of O_2 under visible light ($\lambda > 420$ nm) illumination, producing Cl^- and CO_2 [81]. The ISC formed by the interaction of phenolic compounds with TiO_2 exhibited self-degradation. It was proposed that an electronic transition occurs from the ISC to the C.B. of TiO_2 to form active oxygen species, which also participate in the oxidative degradation of phenolic compounds.

4.3. Interfacial-Surface-Complex-Mediated Visible-Light-Sensitive TiO_2 Photocatalysts

The interfacial surface complex (ISC)-mediated visible-light-sensitive TiO_2 photocatalyst was applied to selective oxidation of several aromatic alcohols [82–88]. Unlike to the ISC in Figure 14, reactant molecules adsorbed onto the TiO_2 surface (ISC) is activated under visible-light irradiation, and they are converted into products. Figure 15 shows reaction time profiles for the oxidation of

benzyl alcohol in an acetonitrile solution suspended with TiO_2 photocatalyst in the presence of O_2 under visible light irradiation ($\lambda > 420$ nm). This reaction does not proceed without TiO_2 or irradiation. It was found that the amount of benzyl alcohol decreased with an increase in the irradiation time, while the amount of benzaldehyde increased. Neither benzoic acid nor CO_2 were formed as oxidative products. The yield of benzaldehyde reached circa 95%, and the carbon balance in the liquid phase was circa 95% after photo-irradiation for 4 h.

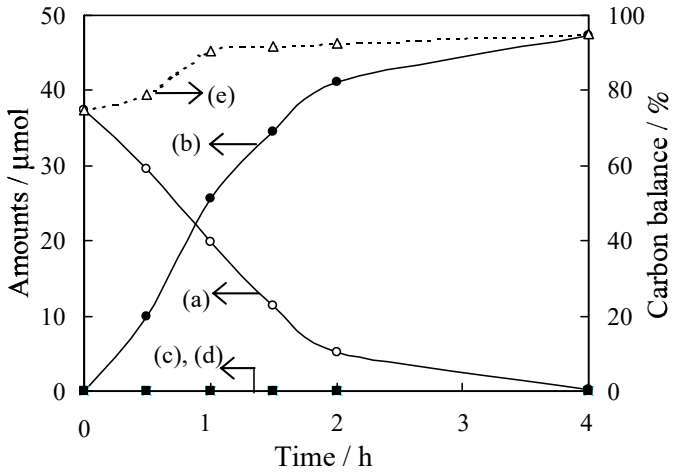

Figure 15. Selective oxidation of benzyl alcohol on TiO_2 (50 mg) under visible light irradiation [82]. The initial amount of benzyl alcohol was 50 μmol. Amounts of: benzyl alcohol (a); benzaldehyde (b); benzoic acid (c); CO_2 (d); and percentage of total organic compounds in solution (e).

Photocatalytic oxidation of benzyl alcohol and its derivatives into corresponding aldehydes was carried out with TiO_2 under visible light irradiation. Benzyl alcohol and its derivatives substituted by $–OCH_3$, –Cl, $–NO_2$, $–CH_3$, $–CF_3$, and $–C(CH_3)_3$ groups were successfully converted to corresponding aldehydes with a high conversion and high selectivity on TiO_2, while no other products were observed (See Table 4). However, the phenolic compound (entry 9) was deeply oxidized, since it strongly adsorbed on the TiO_2 surface [82].

Table 4. Chemoselective photocatalytic oxidation of different kinds of benzylic alcohols on TiO_2 [82].

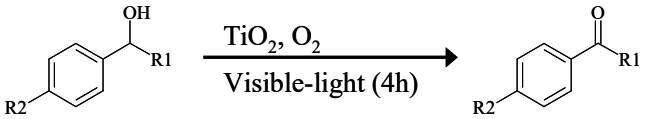

Entry	R_1	R_2	Conversion (%)	Selectivity (%)
1	H	H	> 99	> 99
2	H	$C(CH_3)_3$	> 99	> 99
3	H	OCH_3	> 99	> 99
4	H	CH_3	> 99	> 99
5	H	Cl	> 99	> 99
6	H	NO_2	> 99	> 99
7	H	CF_3	> 99	> 99
8	CH_3	H	> 99	> 99
9	H	OH	> 85	23

4.3.1. What Is the Origin of the Visible Light Response?

The interaction of benzyl alcohol with TiO_2 was analyzed by FT-IR spectroscopy (See Figure 16). Characteristic features of the ISC are as follows: (i) a remarkable downward negative band at 3715 cm^{-1} attributed to the O–H stretching of the terminal OH group; (ii) a new band appeared at circa 1100 cm^{-1},

which is attributed to the C–O stretching of the alkoxide species formed by the interaction of benzyl alcohol with TiO_2, while that of benzyl alcohol by itself is 1020 cm^{-1}.

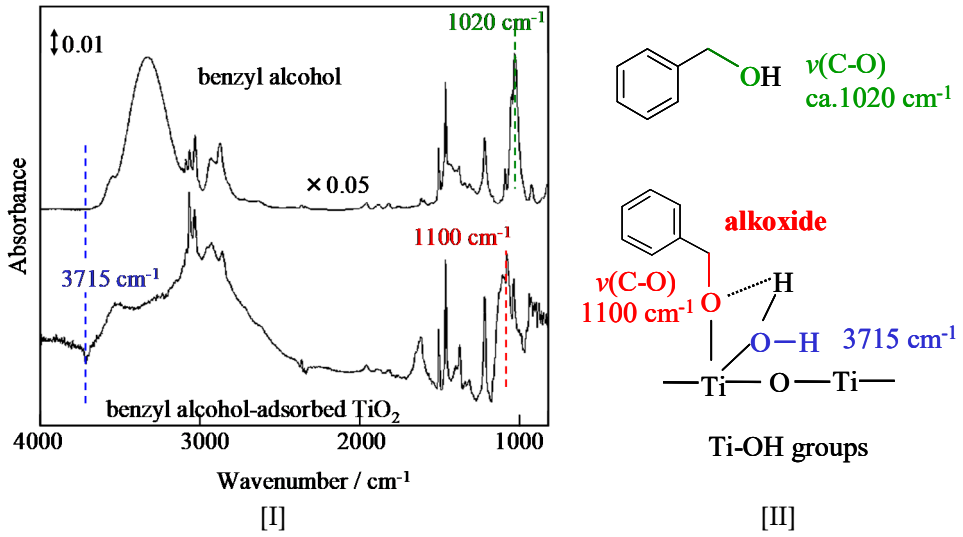

Figure 16. FT-IR spectra [I] of benzyl alcohol by itself and benzyl alcohol adsorbed on TiO_2; and [II] their peak identification [82].

When the TiO_2 was treated by diluted HF (aq), the IR band at 3715 cm^{-1} on the HF–TiO_2 drastically decreased, while the photocatalytic activity significantly decreased. The active sites were confirmed to be alkoxide by the interaction of benzyl alcohol with the terminal OH groups of TiO_2.

TiO_2 by itself exhibited absorption only in the UV region, which is attributed to the charge transition from V.B. to C.B. When the benzyl alcohol was adsorbed on TiO_2, absorption in the visible region could be observed. This absorption in the visible light region is assignable to the ISC through the LMCT (See Figure 17). The action spectra of apparent quantum yield (AQY) plots were fitted with the photo-absorption of TiO_2-adsorbed benzyl alcohol, suggesting that visible light absorption directly participated in the photocatalytic reactions.

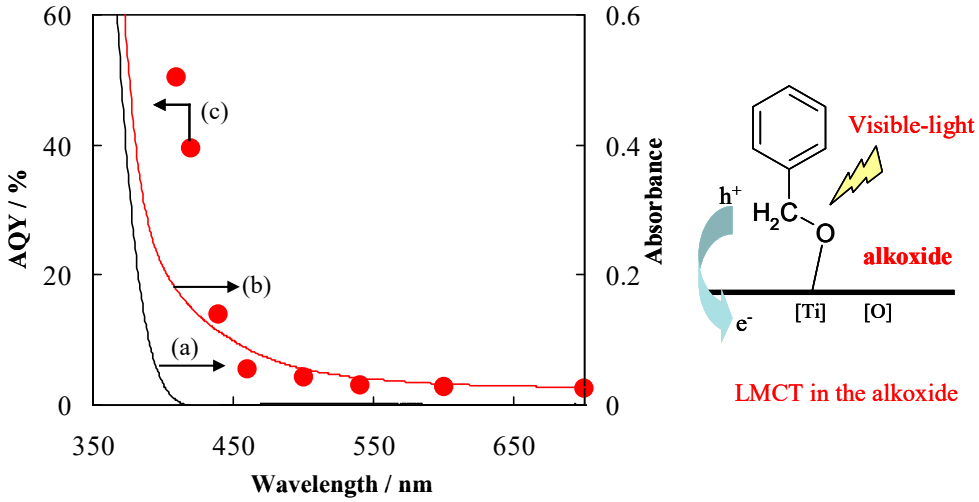

Figure 17. UV-vis absorption spectra of TiO_2 (a), TiO_2 adsorbed with benzyl alcohol (b), and apparent quantum yield (AQY) for the formation of benzaldehyde (c); and schematic illustration of photo-induced charge transfer through LMCT in the alkoxide [82].

DFT calculations [87] indicated the interaction of benzyl alcohol with surface hydroxyl groups on the TiO_2 surface, resulting in the formation of alkoxide species. The electron density contour maps for

the alkoxide species are shown in Figure 18. The orbital #212 at −0.80 eV forms the V.B. of TiO_2, while #218 at +2.25 eV forms the C.B. One type of surface state consisting of the orbital (#215) originates with the alkoxide species ([Ti]–O–CH_2–ph) hybridized with the O2p AOs in the V.B. of the TiO_2. The energy gap between #215 and #218 (2.8 eV) was confirmed to be the origin for the visible light response.

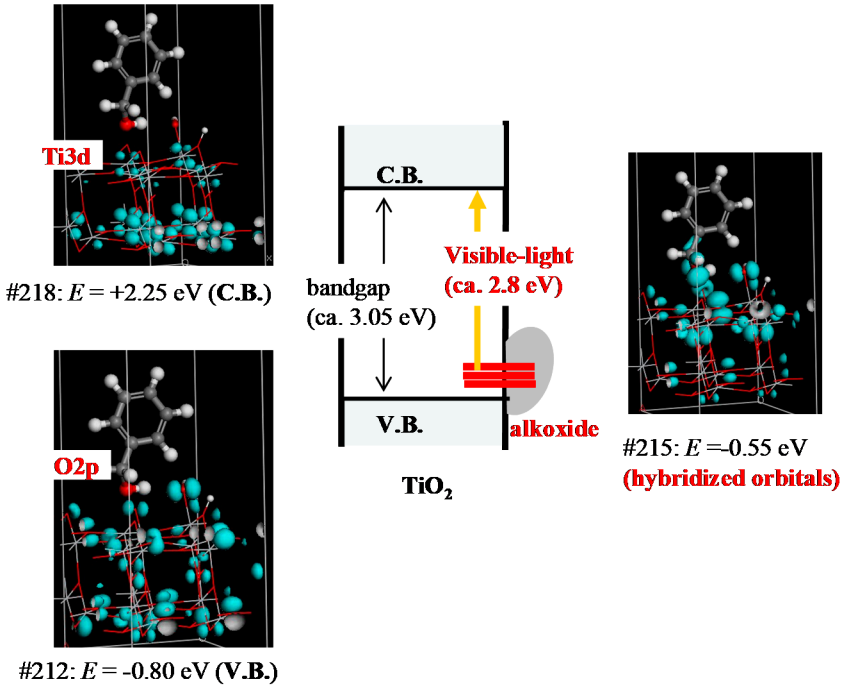

Figure 18. Photo-induced electron transfer from the hybridized orbital to the C.B. of TiO_2 under visible light irradiation [87]. Density maps of V.B., C.B., and hybridized orbital are shown here.

4.3.2. What Makes the High Selectivity for the Photocatalytic Reactions?

It was observed that benzyl alcohol is adsorbed on TiO_2 more favorably than benzaldehyde in a mixture of benzyl alcohol and benzaldehyde under dark conditions. This result indicates that the interaction between benzaldehyde and TiO_2 is fairly weak. According to DFT calculations [87,88], the interaction of benzyl alcohol with the TiO_2 surface formed a hybridized orbital, while benzaldehyde did not form orbital mixing. Therefore, once benzaldehyde was produced by the oxidation of benzyl alcohol, benzaldehyde was immediately released into the bulk solution, and was not oxidized further to benzoic acid or CO_2.

4.3.3. Reaction Mechanisms behind the Selective Photocatalytic Oxidation of Benzyl Alcohol

The photocatalytic activities for the oxidation of benzyl alcohol or α, α-d2 benzyl alcohol were investigated. The kinetic isotope effect (KIE) [$=k_{C\text{-}H}/k_{CD}$] was estimated to be 3.9 at 295 K. This result suggests that the process for the α-deprotonation is the rate determining step (RDS) for the overall reaction. From the experimental and theoretical studies by DFT calculations, one of the favorable reaction paths is depicted in Figure 19. When benzyl alcohol interacts with Ti–OH of the TiO_2, the alkoxide species (ISC) is formed on a Ti site (3). The ISC was photo-excited under visible light irradiation via LMCT of the ISC, which induces holes (h^+) and electrons (e^-). Subsequently, the electrons are transferred to O_2 to form superoxide anions (the bonding distance between O–O becomes longer), which induces α-deprotonation of the benzyl alcohol (4-5TS). Such hydro-peroxide species would further induce the de-protonation from another benzyl alcohol to form benzaldehyde (7-8TS), resulting in regeneration of the surface terminal OH groups. The consecutive generation of the terminal OH groups would, thus, be one of the key factors for the photocatalytic reactions.

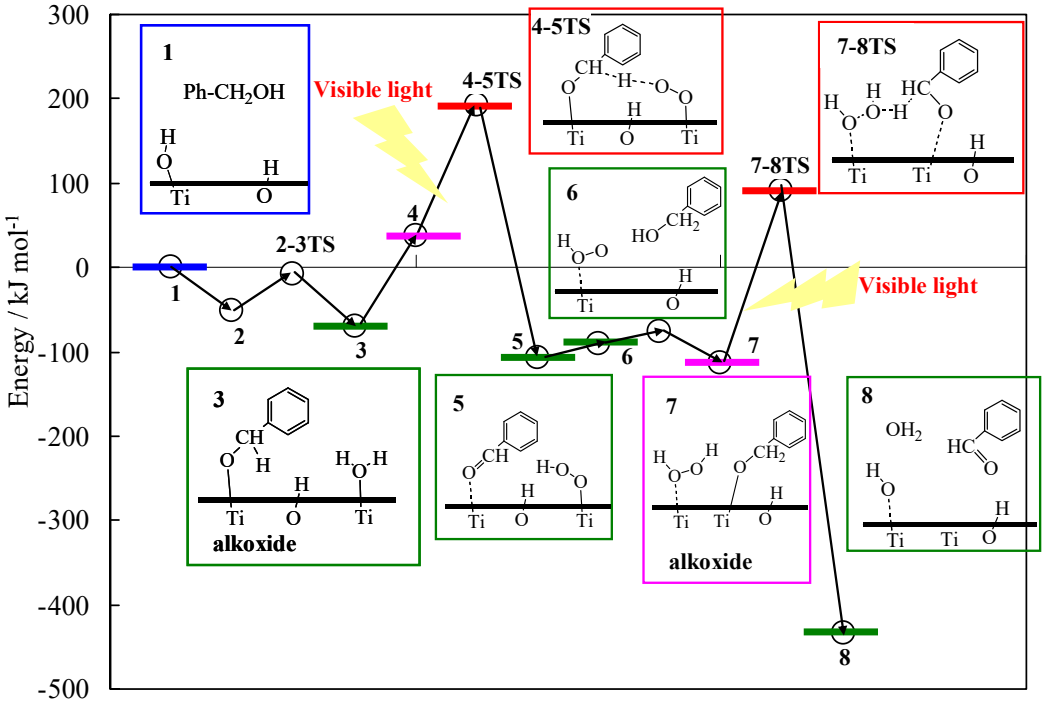

Figure 19. Possible reaction path for the selective oxidation of benzyl alcohol in the presence of O_2 on the TiO_2 under visible light irradiation [87].

4.4. Photocatalytic Oxidation of Benzyl Amine into Imine

Imines are important intermediates for the synthesis of pharmaceuticals and agricultural chemicals. Selective photocatalytic oxidation of benzyl amine into N-benzylidenebenzylamine takes place in the presence of O_2 on the TiO_2 at room temperature (Scheme 1) [89,90]. Several kinds of benzylic amines were examined, and they were converted into the corresponding imines, yielding circa 38–94% [89]. The origin of the visible light response is due to formation of amine oxide (ISC) through the interaction of benzylic amine onto the surface of TiO_2, and the ISC exhibits electronic transition from the localized N 2p orbitals of the amine oxide (ISC) to the C.B. of TiO_2. The photo-induced redox catalysis produces benzaldehyde in the presence of O_2. Subsequently, the condensation reaction of benzaldehyde with another benzyl amine forms N-benzylidenebenzylamine under dark conditions.

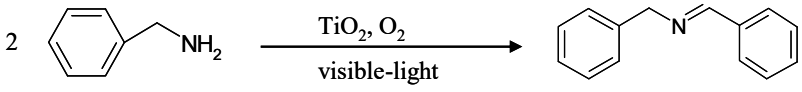

benzyl amine N-benzylidenebenzylamine

Scheme 1. Selective oxidation of benzyl amine into N-benzylidenebenzylamine on the TiO_2 photocatalyst under visible light irradiation.

5. Conclusions

This review focused on some fundamental issues behind the visible-light-sensitive TiO_2 photocatalysts, highlighting the bulk and/or surface electronic structures modified by doping with nitrogen anions; plasmonic Au NPs, and interfacial surface complexes (ISC) and their related photocatalysts. Tailoring the interface and bulk properties, including surface band bending, sub-band structure, surface state distribution, and charge separation, significantly reflects on the photocatalysis. We hope that this review has provided some useful contributions for the future design and development of novel photocatalytic systems employing TiO_2 as well as non-TiO_2 semiconductor materials with nanoscale levels. The applications of such photocatalytic systems could not only convert

unlimited solar energy into chemical energy, but also protect our environment, leading to sustainable green chemistry.

Funding: This research received no external funding.

Conflicts of Interest: The authors declare no conflict of interest.

Abbreviations

NPs	nanoparticles
ISC	interfacial surface complex
VOCs	volatile organic compounds
V.B.	valence band
C.B.	conduction band
XPS	X-ray photoelectron spectroscopy
EPR	electron paramagnetic resonance
UV-vis	Ultraviolet-visible
LSPR	localized surface plasmon resonance
PD	photodeposition
CPH	colloid photodeposition by hole scavenger
DP	deposition precipitation
TEM	transmittance electron microscope
J_{SC}	short-circuit photocurrent
IPCE	incident photo to current efficiency
DFT	density functional theory
MLCT	metal to ligand charge transfer
FT-IR	Fourier transformed-infrared
KIE	kinetic isotope effect
LMCT	ligand to metal charge transfer

References

1. Honda, K.; Fijishima, A. Electrochemical Photolysis of Water at a Semiconductor Electrode. *Nature* **1972**, *238*, 37–38.
2. Inoue, T.; Fujishima, A.; Konishi, S.; Honda, K. Photoelectrocatalytic reduction of carbon dioxide in aqueous suspensions of semiconductor powders. *Nature* **1979**, *277*, 637–638. [CrossRef]
3. Kamat, P.V. Photochemistry on nonreactive and reactive (semiconductor) surfaces. *Chem. Rev.* **1993**, *93*, 267–300.
4. Fox, M.A.; Dulay, M.T. Heterogeneous photocatalysis. *Chem. Rev.* **1993**, *93*, 341–357.
5. Hoffman, M.R.; Martin, S.T.; Choi, W.; Bahnemann, D.W. Environmental applications of semiconductor photocatalysis. *Chem. Rev.* **1995**, *95*, 69–96. [CrossRef]
6. Fujishima, A.; Rao, T.N.; Tryk, A. Titanium dioxide photocatalysis. *J. Photochem. Photobio. C Photochem. Rev.* **2000**, *1*, 1–21. [CrossRef]
7. Anpo, M.; Takeuchi, M. The design and development of highly reactive titanium oxide photocatalysts operating under visible light irradiation. *J. Catal.* **2003**, *216*, 505–516. [CrossRef]
8. Chen, X.; Mao, S.S. Titanium Dioxide Nanomaterials: Synthesis, Properties, Modifications, and Applications. *Chem. Rev.* **2007**, *197*, 2891–2959. [CrossRef]
9. Shiraishi, Y.; Hirai, T. Selective organic transformations on titanium oxide-based photocatalysts. *J. Photochem. Photobiol. C Photochem. Rev.* **2008**, *9*, 157–170. [CrossRef]
10. Palmisano, G.; García-López, E.; Marcì, G.; Loddo, V.; Yurdakal, S.; Augugliaro, V.; Palmisano, L. Advances in selective conversions by heterogeneous photocatalysis. *Chem. Commun.* **2010**, *46*, 7074–7089. [CrossRef]
11. Schneider, J.; Matsuoka, M.; Takeuchi, M.; Zhang, J.; Horiuchi, Y.; Anpo, M.; Bahnemann, D.W. Understanding TiO_2 Photocatalysis: Mechanisms and Materials. *Chem. Rev.* **2014**, *114*, 9919–9986. [CrossRef]
12. Ma, Y.; Wang, X.; Jia, Y.; Chen, X.; Han, H.; Li, C. Titanium dioxide-based nanomaterials for: Photocatalytic fuel generations. *Chem. Rev.* **2014**, *114*, 9987–10043. [CrossRef]

13. Asahi, R.; Morikawa, T.; Irie, H.; Ohwaki, T. Nitrogen-doped titanium dioxide as visiblelight-sensitive photocatalyst: Designs, developments, and prospects. *Chem Rev.* **2014**, *114*, 9824–9852. [CrossRef]
14. Lang, X.; Chen, X.; Zhao, J. Heterogeneous visible light photocatalysis for selective organic transformations. *Chem. Soc. Rev.* **2014**, *43*, 473–486. [CrossRef]
15. Sang, L.; Zhao, Y.; Burda, C. TiO_2 Nanoparticles as Functional Building Blocks. *Chem. Rev.* **2014**, *114*, 9283–9318. [CrossRef]
16. Nosaka, Y.; Nosaka, A.Y. Generation and Detection of Reactive Oxygen Species in Photocatalysis. *Chem. Rev.* **2017**, *117*, 11302–11336. [CrossRef]
17. Kou, J.; Lu, C.; Wang, J.; Chen, Y.; Xu, Z.; Varma, R.S. Selectivity Enhancement in Heterogeneous Photocatalytic Transformations. *Chem. Rev.* **2017**, *117*, 1445–1514. [CrossRef]
18. Prakash, J.; Sun, S.; Swart, H.C.; Gupta, R.K. Noble metals-TiO_2 nanocomposites: From fundamental mechanisms to photocatalysis, surface enhanced Raman scattering and antibacterial applications. *Appl. Mater. Today* **2018**, *11*, 82–135. [CrossRef]
19. Wang, W.; Tadé, M.O.; Shao, Z. Nitrogen-doped simple and complex oxides for photocatalysis: A review. *Prog. Mater. Sci.* **2018**, *92*, 33–63. [CrossRef]
20. Yamashita, H.; Mori, K.; Kuwahara, Y.; Kamegawa, T.; Wen, M.; Verma, P.; Che, M. Single-site and nano-confined photocatalysts designed in porous materials for environmental uses and solar fuels. *Chem. Soc. Rev.* **2018**, *47*, 8072–8096. [CrossRef]
21. Ahmed, A.Y.; Kandiel, T.A.; Oekermann, T.; Bahnemann, D. Photocatalytic Activities of Different Well-defined Single Crystal TiO_2Surfaces: Anatase versus Rutile. *J. Phys. Chem. Lett.* **2011**, *2*, 2461–2465. [CrossRef]
22. Tanaka, K.; Capule, M.F.V.; Hisanaga, T. Effect of Crystallinity of TiO_2 on Its Photo-catalytic Action. *Chem. Phys. Lett.* **1991**, *187*, 73–76. [CrossRef]
23. Luttrell, T.; Halpegamage, S.; Tao, J.; Kramer, A.; Sutter, E.; Batzill, M. Why is anatase a better photocatalyst than rutile? - Model studies on epitaxial TiO_2 films. *Sci. Rep.* **2014**, *4*, 4043–4050. [CrossRef]
24. Gordon, T.R.; Cargnello, M.; Paik, T.; Mangolini, F.; Weber, R.T.; Fornasiero, P.; Murray, C.B. Nonaqueous Synthesis of TiO_2 Nanocrystals Using TiF_4 to Engineer Morphology, Oxygen Vacancy Concentration, and Photocatalytic Activity. *J. Am. Chem. Soc.* **2012**, *134*, 6751–6761. [CrossRef]
25. Zhang, Z.; Wang, C.-C.; Zakaria, R.J.; Ying, Y. Role of Particle Size in Nanocrystalline TiO_2-Based Photocatalysts. *J. Phys. Chem. B* **1998**, *102*, 10871–10878. [CrossRef]
26. Anpo, M.; Ichihashi, Y.; Takeuchi, M.; Yamashita, H. Design of unique titanium oxide photocatalysts by an advanced metal ion-implantation method and photocatalytic reactions under visible light irradiation. *Res. Chem. Intermed.* **1998**, *24*, 143–149. [CrossRef]
27. Sato, S. Photocatalytic activity of NO_x-doped TiO_2 in the visible light region. *Chem. Phys. Lett.* **1986**, *123*, 126–128. [CrossRef]
28. Asahi, R.; Morikawa, T.; Aoki, K.; Taga, Y. Visible-light photocatalysis in nitrogen-doped titanium oxides. *Science* **2001**, *293*, 269–271. [CrossRef]
29. Irie, H.; Watanabe, Y.; Hashimoto, K. Nitrogen-Concentration Dependence on Photocatalytic Activity of $TiO_{2-x}N_x$ Powders. *J. Phys. Chem. B* **2003**, *107*, 5483–5486. [CrossRef]
30. Shin, C.; Bugli, G.; Djega-Mariadassou, G. Preparation and characterization of titanium oxynitrides with high specific surface areas. *J. Solid State Chem.* **1991**, *95*, 145–155. [CrossRef]
31. Livraghi, S.; Paganini, M.C.; Giamello, E.; Selloni, A.; Di Valentin, C.; Pacchioni, G. Origin of Photoactivity of Nitrogen-Doped Titanium Dioxide under Visible Light. *J. Am. Chem. Soc.* **2006**, *128*, 15666–15671. [CrossRef]
32. Wang, J.; Zhu, W.; Zhang, Y.; Liu, S. An efficient two-step technique for nitrogen-doped titanium dioxide synthesizing: Visible-light-induced photodecomposition of methylene blue. *J. Phys. Chem. C* **2007**, *111*, 1010–1014. [CrossRef]
33. Higashimoto, S.; Azuma, M. Photo-induced charging effect and electron transfer to the redox species on nitrogen-doped TiO_2 under visible light irradiation. *Appl. Catal. B Environ.* **2009**, *89*, 557–562. [CrossRef]
34. Wang, H.; Hu, Y. The Photocatalytic Property of Nitrogen-Doped TiO_2 Nanoball Film. *Int. J. Photoenergy* **2013**. [CrossRef]
35. Diwald, O.; Thompson, T.L.; Zubkov, T.; Goralski, E.G.; Walck, S.D.; Yates, J.T., Jr. Photochemical Activity of Nitrogen-Doped Rutile TiO_2(110) in Visible Light. *J. Phys. Chem. B* **2004**, *108*, 6004–6008. [CrossRef]

36. Higashimoto, S.; Ushiroda, Y.; Azuma, M.; Ohue, H. Synthesis, characterization and photocatalytic activity of N-doped TiO_2 modified by platinum chloride. *Catal. Today* **2008**, *132*, 165–169. [CrossRef]
37. Higashimoto, S.; Ushiroda, Y.; Azuma, M. Mechanism for enhancement of visible light response on nitrogen-doped TiO_2 by modification with vanadium species. *J. Nanosci. Nanotechnol.* **2010**, *10*, 246–251. [CrossRef]
38. Nakamura, R.; Tanaka, T.; Nakato, Y. Mechanism for Visible Light Responses in Anodic Photocurrents at N-Doped TiO_2 Film Electrodes. *J. Phys. Chem. B* **2004**, *108*, 10617–10620. [CrossRef]
39. Tang, J.; Cowan, A.J.; Durrant, J.R.; Klug, D.R. Mechanism of O_2 production from water splitting: Nature of charge carriers in nitrogen doped nanocrystalline TiO_2 films and factors limiting O_2 production. *J. Phys. Chem. C* **2011**, *115*, 3143–3150. [CrossRef]
40. Higashimoto, S.; Tanihata, W.; Nakagawa, Y.; Azuma, M.; Ohue, H.; Sakata, Y. Effective photocatalytic decomposition of VOC under visible-light irradiation on N-doped TiO_2 modified by vanadium species. *Appl. Catal. A Gen.* **2008**, *340*, 98–104. [CrossRef]
41. Morikawa, T.; Ohwaki, T.; Suzuki, K.; Moribe, S.; Tero-Kubota, S. Visible-light-induced photocatalytic oxidation of carboxylic acids and aldehydes over N-doped TiO_2 loaded with Fe, Cu or Pt. *Appl. Catal. B Environ.* **2008**, *83*, 56–62. [CrossRef]
42. Sreethawong, T.; Laehsalee, S.; Chavadej, S. Use of Pt/N-doped mesoporous-assembled nanocrystalline TiO_2 for photocatalytic H_2 production under visible light irradiation. *Catal. Commun.* **2009**, *10*, 538–543. [CrossRef]
43. Dolat, D.; Quici, N.; Kusiak-Nejman, E.; Morawski, A.W.; Puma, G.L. One-step, hydrothermal synthesis of nitrogen, carbon co-doped titanium dioxide (N,C-TiO_2) photocatalysts. Effect of alcohol degree and chain length as carbon dopant precursors on photocatalytic activity and catalyst deactivation. *Appl. Catal. B Environ.* **2012**, *115*, 81–89. [CrossRef]
44. Virkutyte, J.; Varma, R.S. Visible light activity of Ag-loaded and guanidine nitrate-doped nano-TiO_2: Degradation of dichlorophenol and antibacterial properties. *RSC Adv.* **2012**, *2*, 1533–1539. [CrossRef]
45. Cong, Y.; Zhang, J.; Chen, F.; Anpo, M. Synthesis and Characterization of Nitrogen-Doped TiO_2Nanophotocatalyst with High Visible Light Activity. *J. Phys. Chem. C* **2007**, *111*, 6976–6982. [CrossRef]
46. Yang, X.; Cao, C.; Erickson, L.; Hohn, K.; Maghirang, R.; Klabunde, K. Synthesis of visible-light-active TiO_2-based photocatalysts by carbon and nitrogen doping. *J. Catal.* **2008**, *260*, 128–133. [CrossRef]
47. Mitoraj, D.; Kisch, H. On the Mechanism of Urea–Induced Titania Modification. *Chem. Eur. J.* **2010**, *16*, 261–269. [CrossRef]
48. Chai, B.; Peng, T.; Mao, J.; Li, K.; Zan, L. Graphitic carbon nitride (g-C_3N_4)-Pt-TiO_2 nanocomposite as an efficient photocatalyst for hydrogen production under visible light irradiation. *Phys. Chem. Chem. Phys.* **2012**, *14*, 16745–16752. [CrossRef]
49. Han, C.; Wang, Y.; Lei, Y.; Wang, B.; Wu, N.; Shi, Q.; Li, Q. *In situ* synthesis of graphitic-C_3N_4 nanosheet hybridized N-doped TiO_2 nanofibers for efficient photocatalytic H_2 production and degradation. *Nano Res.* **2015**, *8*, 1199–1209. [CrossRef]
50. Yan, H.; Yang, H. TiO_2-g-C_3N_4 composite materials for photocatalytic H_2 evolution under visible light irradiation. *J. Alloy. Comp.* **2010**, *509*, L26–L29. [CrossRef]
51. Higashimoto, S.; Hikita, K.; Azuma, M.; Yamamoto, M.; Takahashi, M.; Sakata, Y.; Matsuoka, M.; Kobayashi, H. Visible Light-Induced Photocatalysis on Carbon Nitride Deposited Titanium Dioxide: Hydrogen Production from Sacrificial Aqueous Solutions. *Chin. J. Chem.* **2017**, *35*, 165–172. [CrossRef]
52. Zhang, Q.; Gangadharan, D.T.; Liu, Y.; Xu, Z.; Chaker, M.; Ma, D. Recent advancements in plasmon-enhanced visible light-driven water splitting. *J. Materiomics* **2017**, *3*, 33–50. [CrossRef]
53. Ohko, Y.; Tatsuma, T.; Fujii, T.; Naoi, K.; Niwa, C.; Kubota, Y.; Fujishima, A. Multicolour photochromism of TiO_2 films loaded with silver nanoparticles. *Nat. Mater.* **2003**, *2*, 29–31. [CrossRef] [PubMed]
54. Tian, Y.; Tatsuma, T. Plasmon-induced photoelectrochemistry at metal nanoparticles supported on nanoporous TiO_2. *Chem. Commun.* **2004**, *0*, 1810–1811. [CrossRef] [PubMed]
55. Tian, Y.; Tatsuma, T. Mechanisms and Applications of Plasmon-Induced Charge Separation at TiO_2 Films Loaded with Gold Nanoparticles. *J. Am. Chem. Soc.* **2005**, *127*, 7632–7637. [CrossRef] [PubMed]
56. Kowalska, E.; Abe, R.; Ohtani, B. Visible light-induced photocatalytic reaction of gold-modified titanium(IV) oxide particles: Action spectrum analysis. *Chem. Commun.* **2009**, *0*, 241–243. [CrossRef] [PubMed]

57. Kowalska, E.; Mahaney, O.O.P.; Abe, R.; Ohtani, B. Visible-light-induced photocatalysis through surface plasmon excitation of gold on titania surfaces. *Phys. Chem. Chem. Phys.* **2010**, *12*, 2344–2355. [CrossRef] [PubMed]
58. Kolinko, P.A.; Selishchev, D.S.; Kozlov, D.V. Visible Light Photocatalytic Oxidation of Ethanol Vapor on Titanium Dioxide Modified with Noble Metals. *Theor. Exp. Chem.* **2015**, *51*, 96–103. [CrossRef]
59. Frens, G. Controlled Nucleation for the Regulation of the Particle Size in Monodisperse Gold Suspensions. *Nat. Phys. Sci.* **1973**, *241*, 20–22. [CrossRef]
60. Tanaka, A.; Ogino, A.; Iwaki, M.; Hashimoto, K.; Ohnuma, A.; Amano, F.; Ohtani, B.; Kominami, H. Gold–Titanium(IV) Oxide Plasmonic Photocatalysts Prepared by a Colloid-Photodeposition Method: Correlation Between Physical Properties and Photocatalytic Activities. *Langmuir* **2012**, *28*, 13105–13111. [CrossRef]
61. Silva, C.G.; Juarez, R.; Marino, T.; Molinari, R.; Garcia, H. Influence of Excitation Wavelength (UV or Visible Light) on the Photocatalytic Activity of Titania Containing Gold Nanoparticles for the Generation of Hydrogen or Oxygen from Water. *J. Am. Chem. Soc.* **2011**, *133*, 595–602. [CrossRef] [PubMed]
62. Zanella, R.; Delannoy, L.; Louis, C. Mechanism of deposition of gold precursors onto TiO_2 during the preparation by cation adsorption and deposition–precipitation with NaOH and urea. *Appl. Catal. A Gen.* **2005**, *291*, 62–72. [CrossRef]
63. Tanaka, A.; Sakaguchi, S.; Hashimoto, K.; Kominami, H. Preparation of Au/TiO_2 with Metal Cocatalysts Exhibiting Strong Surface Plasmon Resonance Effective for Photoinduced Hydrogen Formation under Irradiation of Visible Light. *ACS Catal.* **2013**, *3*, 79–85. [CrossRef]
64. Tanaka, A.; Nakanishi, K.; Hamada, R.; Hashimoto, K.; Kominami, H. Simultaneous and Stoichiometric Water Oxidation and Cr(VI) Reduction in Aqueous Suspensions of Functionalized Plasmonic Photocatalyst Au/TiO_2–Pt under Irradiation of Green Light. *ACS Catal.* **2013**, *3*, 1886–1891. [CrossRef]
65. Tanaka, A.; Nishino, Y.; Sakaguchi, S.; Yoshikawa, T.; Imamura, K.; Hashimoto, K.; Kominami, H. Functionalization of a plasmonic Au/TiO_2 photocatalyst with an Ag co-catalyst for quantitative reduction of nitrobenzene to aniline in 2-propanol suspensions under irradiation of visible light. *Chem. Commun.* **2013**, *49*, 2551–2553. [CrossRef] [PubMed]
66. Tanaka, A.; Hashimoto, K.; Kominami, H. A very simple method for the preparation of Au/TiO_2 plasmonic photocatalysts working under irradiation of visible light in the range of 600–700 nm. *Chem. Commun.* **2017**, *53*, 4759–4762. [CrossRef]
67. Naya, S.; Teranishi, M.; Isobe, T.; Tada, H. Light wavelength-switchable photocatalytic reaction by gold nanoparticle-loaded titanium(IV) dioxide. *Chem. Commun.* **2010**, *46*, 815–817. [CrossRef]
68. Naya, S.; Kimura, K.; Tada, H. One-Step Selective Aerobic Oxidation of Amines to Imines by Gold Nanoparticle-Loaded Rutile Titanium(IV) Oxide Plasmon Photocatalyst. *ACS Catal.* **2013**, *3*, 10–13. [CrossRef]
69. Tsukamoto, D.; Shiraishi, Y.; Sugano, Y.; Ichikawa, S.; Tanaka, S.; Hirai, T. Gold Nanoparticles Located at the Interface of Anatase/Rutile TiO_2 Particles as Active Plasmonic Photocatalysts for Aerobic Oxidation. *J. Am. Chem. Soc.* **2012**, *134*, 6309–6315. [CrossRef]
70. Zheng, Z.; Huang, B.; Qin, X.; Zhang, X.; Dai, Y.; Whangbo, M.-H. Facile *in situ* synthesis of visible-light plasmonic photocatalysts $M@TiO_2$ (M = Au, Pt, Ag) and evaluation of their photocatalytic oxidation of benzene to phenol. *J. Mater. Chem.* **2011**, *21*, 9079–9087. [CrossRef]
71. Tanaka, A.; Sakaguchi, S.; Hashimoto, K.; Kominami, H. Preparation of Au/TiO_2 exhibiting strong surface plasmon resonance effective for photoinduced hydrogen formation from organic and inorganic compounds under irradiation of visible light. *Catal. Sci. Technol.* **2012**, *2*, 907–909. [CrossRef]
72. Tanaka, A.; Teramura, K.; Hosokawa, S.; Kominami, H.; Tanaka, T. Visible light-induced water splitting in an aqueous suspension of a plasmonic Au/TiO_2 photocatalyst with metal co-catalysts. *Chem. Sci.* **2017**, *8*, 2574–2580. [CrossRef] [PubMed]
73. Furube, A.; Du, L.; Hara, K.; Katoh, R.; Tachiya, M. Ultrafast Plasmon-Induced Electron Transfer from Gold Nanodots into TiO_2 Nanoparticles. *J. Am. Chem. Soc.* **2007**, *129*, 14852–14853. [CrossRef] [PubMed]
74. Borgarello, E.; Kiwi, J.; Pelizzetti, E.; Visca, M.; Grätzel, M. Photochemical cleavage of water by photocatalysis. *Nature* **1981**, *289*, 158–160. [CrossRef]
75. Vinodgopal, K.; Hua, X.; Dahlgren, R.L. Photochemistry of $Ru(bpy)_2(dcbpy)^{2+}$ on $A1_2O_3$ and TiO_2 surfaces. an insight into the mechanism of photosensitization. *J. Phys. Chem.* **1995**, *99*, 10883–10889. [CrossRef]

76. Sakthivel, S.; Kisch, H. Daylight photocatalysis by carbon-modified titanium dioxide. *Angew. Chem. Int. Ed.* **2003**, *42*, 4908–4911. [CrossRef] [PubMed]
77. Macyk, W.; Burgeth, G.; Kisch, H. Photoelectrochemical properties of platinum(IV) chloride surface modified TiO_2. *Photochem. Photobiol. Sci.* **2003**, *2*, 322–328. [CrossRef]
78. Higashimoto, S.; Nishi, T.; Yasukawa, M.; Azuma, M.; Sakata, Y.; Kobayashi, H. Photocatalysis of titanium dioxide modified by interfacial surface complexes (ISC) with different substituted groups. *J. Catal.* **2015**, *329*, 286–290. [CrossRef]
79. Ikeda, S.; Abe, C.; Torimoto, T.; Ohtani, B. Photochemical hydrogen evolution from aqueous triethanolamine solutions sensitized by binaphthol-modified titanium(IV) oxide under visible-light irradiation. *J. Photochem. Photobiol. A Chem.* **2003**, *160*, 61–67. [CrossRef]
80. Kamegawa, T.; Seto, H.; Matsuura, S.; Yamashita, H. Preparation of hydroxynaphthalene modified TiO_2 via formation of surface complexes and their applications in the photocatalytic reduction of nitrobenzene under visible-light irradiation. *ACS Appl. Mater. Interfaces* **2012**, *4*, 6635–6639. [CrossRef]
81. Kim, S.; Choi, W. Visible-light-induced photocatalytic degradation of 4-chlorophenol and phenolic compounds in aqueous suspension of pure titania: Demonstrating the existence of a surface-complex-mediated path. *J. Phys. Chem. B* **2005**, *109*, 5143–5149. [CrossRef] [PubMed]
82. Higashimoto, S.; Kitao, N.; Yoshida, N.; Sakura, T.; Azuma, M.; Ohue, H.; Sakata, Y. Selective photocatalytic oxidation of benzyl alcohol and its derivatives into corresponding aldehydes by molecular oxygen on titanium dioxide under visible light irradiation. *J. Catal.* **2009**, *266*, 279–285. [CrossRef]
83. Higashimoto, S.; Okada, K.; Morisugi, T.; Azuma, M.; Ohue, H.; Kim, T.-H.; Matsuoka, M.; Anpo, M. Effect of surface treatment on the selective photocatalytic oxidation of benzyl alcohol infrared study of hydroxy groups on coordinative defect sites. *Top. Catal.* **2010**, *53*, 578–583. [CrossRef]
84. Higashimoto, S.; Okada, K.; Azuma, M.; Ohue, H.; Terai, T.; Sakata, Y. Characteristics of the charge transfer surface complex on titanium(IV) dioxide for the visible light induced chemoselective oxidation of benzyl alcohol. *RSC Adv.* **2012**, *2*, 669–676. [CrossRef]
85. Higashimoto, S.; Suetsugu, N.; Azuma, M.; Ohue, H.; Sakata, Y. Efficient and selective oxidation of benzylic alcohol by O_2 into corresponding aldehydes on a TiO_2 photocatalyst under visible light irradiation: Effect of phenyl-ring substitution on the photocatalytic activity. *J. Catal.* **2010**, *274*, 76–83. [CrossRef]
86. Higashimoto, S.; Shirai, R.; Osano, Y.; Azuma, M.; Ohue, H.; Sakata, Y.; Kobayashi, H. Influence of metal ions on the photocatalytic activity: Selective oxidation of benzyl alcohol on iron (III) ion-modified TiO_2, using visible light. *J. Catal.* **2014**, *311*, 137–143. [CrossRef]
87. Kobayashi, H.; Higashimoto, S. DFT study on the reaction mechanisms behind the catalytic oxidation of benzyl alcohol into benzaldehyde by O_2 over anatase TiO_2 surfaces with hydroxyl groups: Role of visible-light irradiation. *Appl. Catal. B Environ.* **2015**, *170*, 135–143. [CrossRef]
88. Li, R.; Kobayashi, H.; Guo, J.; Fan, J. Visible-light induced high-yielding benzyl alcohol-to benzaldehyde transformation over mesoporous crystalline TiO_2: A self-adjustable photooxidation system with controllable hole-generation. *J. Phys. Chem. C* **2011**, *115*, 23408–23416. [CrossRef]
89. Lang, X.; Ma, W.; Zhao, Y.; Chen, C.; Ji, H.; Zhao, J. Visible-light-induced selective catalytic aerobic oxidation of amines into imines on TiO_2. *Chem. Eur. J.* **2012**, *18*, 2624–2631. [CrossRef]
90. Higashimoto, S.; Hatada, Y.; Ishikawa, R.; Azuma, M.; Sakata, Y.; Kobayashi, H. Selective Photocatalytic Oxidation of Benzyl Amine by O_2 into N-Benzylidenebenzylamine on TiO_2 Using Visible Light. *Curr. Org. Chem.* **2013**, *17*, 2374–2381. [CrossRef]